Proceedings of the
Annual Stability Conference
Structural Stability Research Council
Louisville, Kentucky, April 13-16, 2021

Imperfection sensitivity of metallic plate-lattice materials

Fani Derveni[1], Andrew Gross[2], Kara D. Peterman[3], Simos Gerasimidis[4]

Abstract
As system design objectives move towards effective lightweight construction, innovative materials of high strength, stiffness, stability, and energy absorption have received significant attention. Recent advances in 3D printing empower this effort, since they enable fabrication of complex cellular architectures with beneficial properties, called architected materials. Besides the solid constituent material, the mechanical properties of architected materials are primarily determined by their geometry. Very recently it was discovered that a new generation of architected materials composed of plates, called plate-lattice materials, can achieve the theoretical strength and stiffness upper bounds, exceeding the properties of any previously investigated architected materials. This work focuses on the stability of metallic imperfect plate-lattices of five different architectures under compressive loading and aims to provide new knockdown factors. This is accomplished via three-dimensional shell finite element models of isotropic and anisotropic geometries with periodic boundary conditions. The buckling behavior and corresponding modal shapes are obtained through unit cell simulations, as well as through tessellations of unit cells to capture long buckling wavelengths. Finally, an imperfection sensitivity analysis is conducted by using geometric imperfections incorporated in the computational model based on the modal shapes. This study characterizes the behavior and stability of new generation design materials for use in structural applications.

1. Introduction

Architected materials are cellular materials whose behavior is mainly governed by their geometry instead of their constituent material. The progress of additive manufacturing enhances the ability of 3D printing new, lightweight materials with advantageous properties in terms of stiffness, strength, energy absorption, and stability. Cellular architected materials can be classified as foams, truss-lattices, shell-lattices, and plate-lattices, which can be governed by bending- or stretching-dominated behavior.

[1] PhD Candidate, University of Massachusetts, Amherst, <fderveni@umass.edu>
[2] Assistant Professor, University of South Carolina, < andrewgross@sc.edu >
[3] Assistant Professor, University of Massachusetts, Amherst, <kdpeterman@umass.edu>
[4] Assistant Professor, University of Massachusetts, Amherst, < sgerasimidis@umass.edu >

The mechanical performance of foams and/or honeycombs has been extensively examined by multiple researchers (Gibson et al. 1982, Gibson and Ashby 1982, Papka and Kyriakides 1999, Deshpande and Fleck 2000), and have demonstrated that foams are governed by high energy absorption properties and high stiffness. Bending- versus stretching-dominated foams have been investigated (Deshpande et al. 2001) by assessing their strength-to-weight ratios. Due to their closed-cell structure, honeycombs have limitations in the lower relative density ranges.

Numerous research efforts have been conducted on truss-lattices, and specifically the octet-truss (Deshpande et al. 2001, Elsayed and Pasini 2010, Gu and Greer 2015, Gross et al. 2019), showing that truss-lattices are stronger and stiffer than foams especially for lower relative densities due to their open-cell geometry. Fracture toughness of the octet truss has been also studied (O'Masta et al. 2017) by testing titanium lattice structures, while hierarchical materials have been tested and simulated (Meza et al. 2015) using the octahedron and the octet-truss.

Recent studies on smooth-shell lattice materials have been also conducted (Bonatti and Mohr 2019, Bonatti and Mohr 2019) focusing mainly on Triply Periodic Minimal Surface (TPMS-like) structures and showing the advantageous elastic properties of smooth-shell lattices in comparison to truss-lattice materials of the same relative density using optimization, computational and experimental methods. Low-density shellular structures have also been experimentally evaluated (Han et al. 2015, Han and Kang 2019) indicating the advantageous response of shellular structures.

Plate-lattice materials have been recently investigated (Berger et al. 2017, Tancogne-Dejean et al. 2018) showing that plate-lattices of cubic symmetry are able to reach the theoretical stiffness bound (Hashin Shtrikman bound (Hashin and Shtrikman 1963)) for isotropic materials and they are the stiffest existing cellular materials to the authors' knowledge. Isotropic plate-lattices are analytically proposed by combining the Simple Cubic (SC) geometry with the Face-Centered Cubic (FCC) and/or Body-Centered Cubic (BCC). Strength has also been examined (Crook et al. 2020), concluding that plate-lattices are able to reach the theoretical strength bound (Suquet bound) through experimental and computational work. Furthermore, the impact of strain rate in the strength and failures of plate-lattices has been evaluated (Tancogne-Dejean et al. 2019). Even though stiffness and strength have been approached by many researchers, the stability and imperfection sensitivity of plate-lattices has not been explored yet.

This work aims to provide innovative results on the stability of plate-lattices of cubic symmetry and to provide accurate knockdown factors. Five architectures of cubic symmetry are adopted (SC, BCC, FCC, SC-BCC, SC-FCC) and a relative density $\rho^*=25\%$ is used to evaluate the stability of these structures. Perfect and imperfect architectures are examined and knockdown factors for all architectures are proposed. In addition, relative densities between 25% and 3% are examined for the SC geometry aiming to give insight of the imperfection sensitivity of ultra-thin plates and the different failure modes that govern each case. Finite element models are used in this study and geometric imperfections are included as modal shapes. The main focus of this work is to assess and understand the behavior of new materials that can potentially improve the performance of different structural applications that require high strength, stiffness and stability in comparison to the existing state-of-the-art structural materials. These materials can potentially enhance lightweight construction with resilient and imperfection insensitive material options that can be used as infrastructure repair solutions, connecting elements and energy dissipating mechanisms.

2. Plate-lattice materials

Plate-lattice mechanical metamaterials of cubic symmetry are the focus of this work. The plate-lattices are composed of plates, and specifically of plates located in a manner analogous to common crystal structures. The plate-lattice architectures are adopted from Berger et al. (2017) and Tancogne-Dejean et al. (2018).

2.1 Geometry

Five plate-lattice geometries are used including three anisotropic architectures and two isotropic combinations. The anisotropic plate lattices are the Simple Cubic (SC), the Body-Centered Cubic (BCC), and the Face-Centered Cubic (FCC), while the isotropic architectures are obtained by combining the anisotropic geometries such as SC-BCC and SC-FCC. The schematic representation of the plate-lattice architectures examined herein is illustrated in Fig. 1. To obtain isotropic geometries, thickness ratios as analytically described by Berger et al. (2017) and Tancogne-Dejean et al. (2018) are defined in Eq. 1 and Eq. 2 for SC-FCC and SC-BCC respectively.

$$t_{FCC} = \frac{9t_{SC}}{8\sqrt{3}} \tag{1}$$

where t_{SC} is the SC plate thickness and t_{FCC} is FCC plate thickness.

$$t_{BCC} = t_{SC}\sqrt{2} \tag{2}$$

where t_{SC} is the SC plate thickness and t_{BCC} is BCC plate thickness.

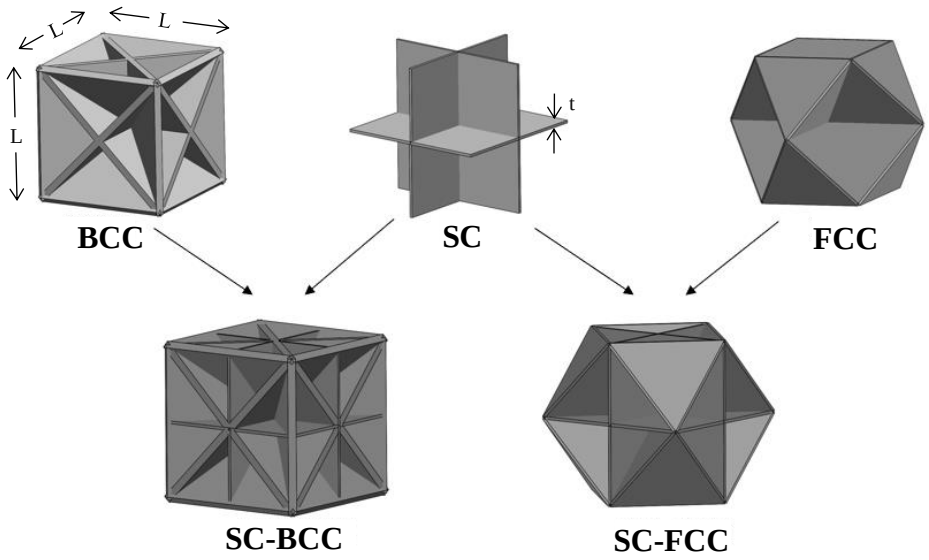

Figure 1: Geometry representation of anisotropic (SC, BCC, FCC) and isotropic (SC-BCC, SC-FCC) plate-lattice materials. The unit-cell length L is constant for all geometries, while thickness t varies between the architectures.

A relative density of $\rho^*=25\%$ is chosen herein calculated as the volume fraction of the volume of the solid to the volume of the whole unit-cell. Since some of the geometries are braced with more plates than others, $\rho^*=25\%$ does not correspond to equal thicknesses in all geometries. The

thickness of all geometries is summarized in Table 1. The unit-cell length is constant and equal to L=16.404 mm.

Table 1: Thickness of plate-lattices of ρ*=25%

Plate-Lattice Architecture	Thickness (mm) t_{SC}	t_{BCC}	t_{FCC}
SC	1.367	-	-
BCC	-	0.483	-
FCC	-	-	0.592
SC-BCC	0.273*	0.387	-
SC-FCC	0.547	-	0.355*

*Minimum thickness t used for the different imperfection amplitudes.

2.2 Tessellation dependency and imperfection amplitude

This work focuses on both perfect and imperfect geometries. The selected imperfection amplitudes for all the imperfect plate-lattices are 0.1t, 0.5t, 1t, and 2t, where t is the minimum thickness of each geometry. The imperfections herein are introduced as modal shapes based on the first eigenmode. The modal shapes are obtained via linear elastic analyses under uniaxial compression using the finite element software Abaqus (Abaqus 2018). The obtained eigenmode shapes that are used to define imperfect geometries are shown in the inset figures in Fig. 2 for all plate-lattice material architectures. The contours in the inset figures represent displacements (magnitude) of the first eigenmode.

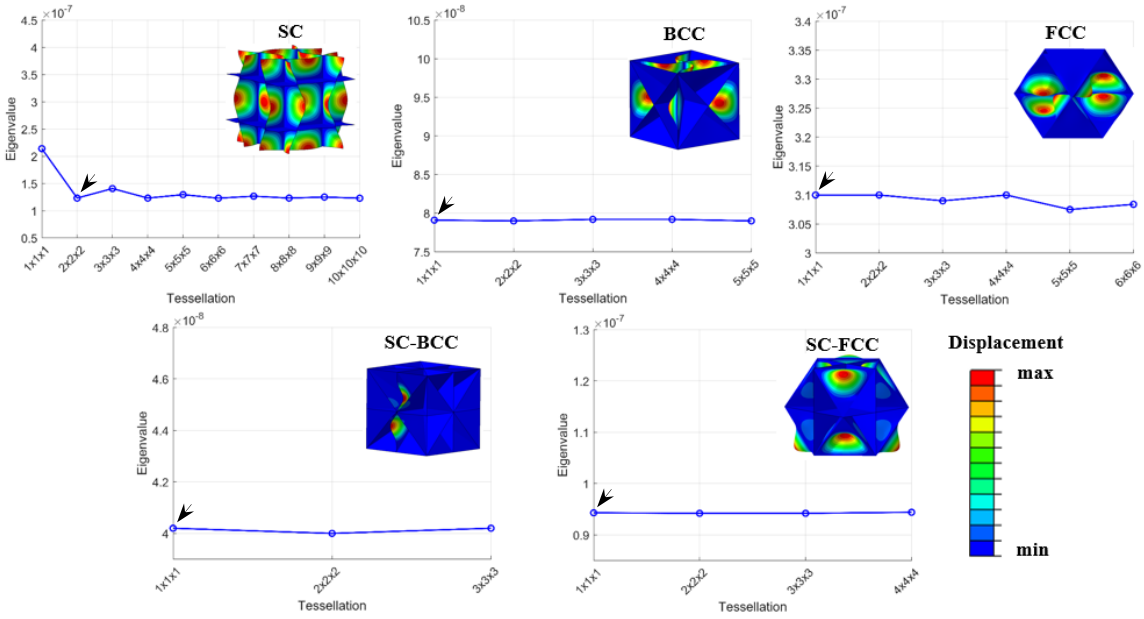

Figure 2: Tessellation dependency for SC, BCC, FCC, SC-BCC, and SC-FCC plate-lattice materials. A 2x2x2 tessellation is selected for SC, while a 1x1x1 unit-cell is selected for all remaining geometries (indicated by arrows). First eigenmode shapes of all geometries are included as inset figures.

A tessellation dependency study is conducted based on the first eigenvalue and eigenmode in order to capture long wavelength buckling effects (material properties and boundary conditions are

described in the following section). The results shown in Fig. 2 (first eigenvalue against tessellation number), recommend that SC geometry is governed by buckling with a wavelength twice that of the unit cell and that a 2x2x2 tessellation is able to capture the behavior of the plate-lattice, while FCC, BCC, SC-FCC, and SC-BCC are not governed by long wavelength buckling, and thus a 1x1x1 unit-cell is selected.

3. Finite element modeling approach

A computational modeling approach is used for SC, BCC, FCC, SC-BCC, and SC-FCC using finite element software Abaqus (Abaqus 2018). Mesh, material properties, imperfections, boundary conditions, and loading are described herein.

3.1 Mesh Discretization and Material Properties

Shell elements are used from Abaqus library, and specifically four-node S4 elements are selected. Mesh convergence is conducted and a mesh size of 0.3mm is chosen for all plate-lattice architectures (SC, BCC, FCC, SC-BCC, SC-FCC). Fig. 3 shows the mesh convergence results for all architectures for the first eigenvalue (ratio of first eigenvalue (Eigenvalue 1) normalized by the exact value ($Eigen1_{exact}$) against ratio of 1 over the mesh size).

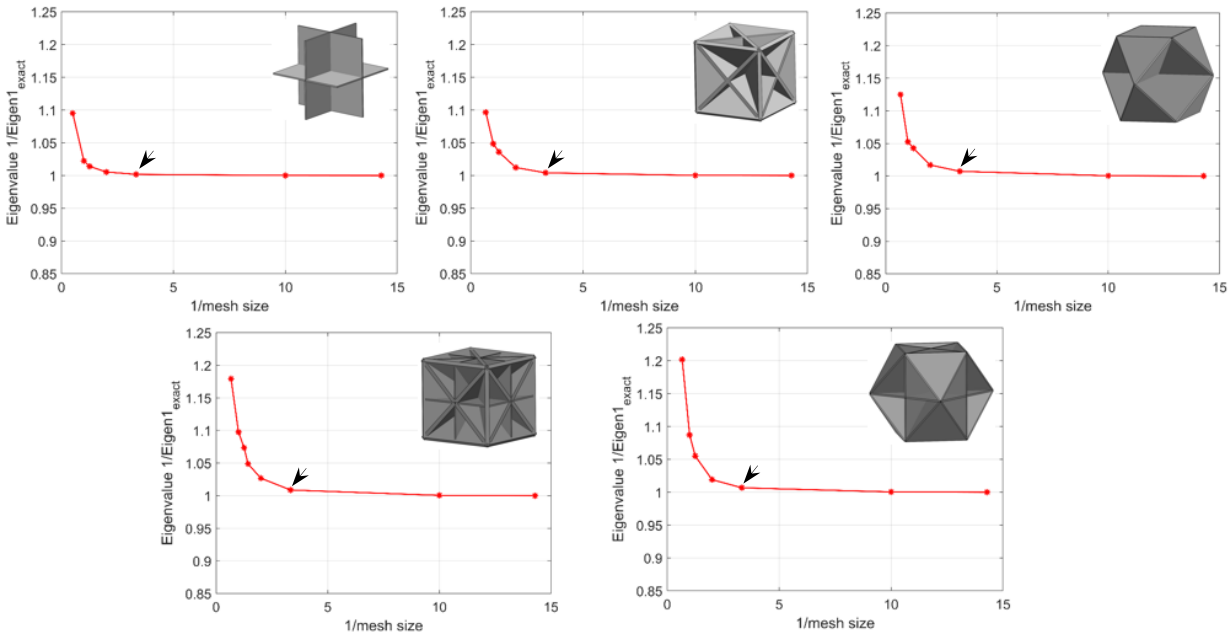

Figure 3: Mesh convergence for SC, BCC, FCC, SC-BCC, and SC-FCC plate-lattice materials. A mesh size of 0.3mm is selected for all geometries, as indicated with the arrows.

The base material is chosen as 316L stainless steel powder and it is simulated as elastic perfectly plastic. The Young's modulus is equal to E=200GPa, the Poisson's ratio is v=0.3, and the yield strength is equal to σ_y=1000MPa. The density is equal to ρ=7.8g/cc.

3.2 Loading and Boundary Conditions

Uniaxial compression is applied to all architectures using an applied strain rate equal to 0.01/sec. Static General, Static Riks, and Dynamic Implicit analyses resulted to the same behavior in terms

of strength, stiffness and failures for high relative densities, while for lower relative densities (as examined in Results and Discussion section) static analyses could not accurately capture the behavior of plate-lattices, and thus Dynamic Implicit solver is used herein by selecting the Quasi-Static application and a Smooth Step Amplitude. For low relative densities, the strain rate is reduced to 0.0004/sec with a time period of 50sec, an initial and maximum step of 0.005, and a minimum step of 10^{-10}. A stiffness damping coefficient of 0.001 is used to reduce computational cost, while has negligible impact on the response of the plate-lattices and provides accurate results.

Periodic boundary conditions are used to eliminate finite size effects. Virtual nodes are introduced using equation constraints, and kinematic constraints are applied on sets of matching nodes in the lattice boundaries.

4. Results and Discussion

The finite element modeling results are discussed herein focusing on the stress-strain response of SC, BCC, FCC, SC-BCC, and SC-FCC plate-lattices of ρ*=25%, as well as on their governing failure mechanisms. The effect of smaller relative-density materials is also approached for representation for the SC geometry.

4.1 Strength, Failures, and Knockdown Factors

The first finding of this work is that all SC, BCC, FCC, SC-FCC, and SC-BCC plate-lattices are imperfection sensitive for ρ*=25%. The results in Fig. 4 illustrate macroscopic stress-strain curves for different imperfection amplitudes between 0t and 2t showing that imperfection amplitude increase leads to strength decrease. Given that thickness is not the same for all geometries of ρ*=25%, the comparison between the different geometries does not reveal significant differences in terms of capacity and failure modes.

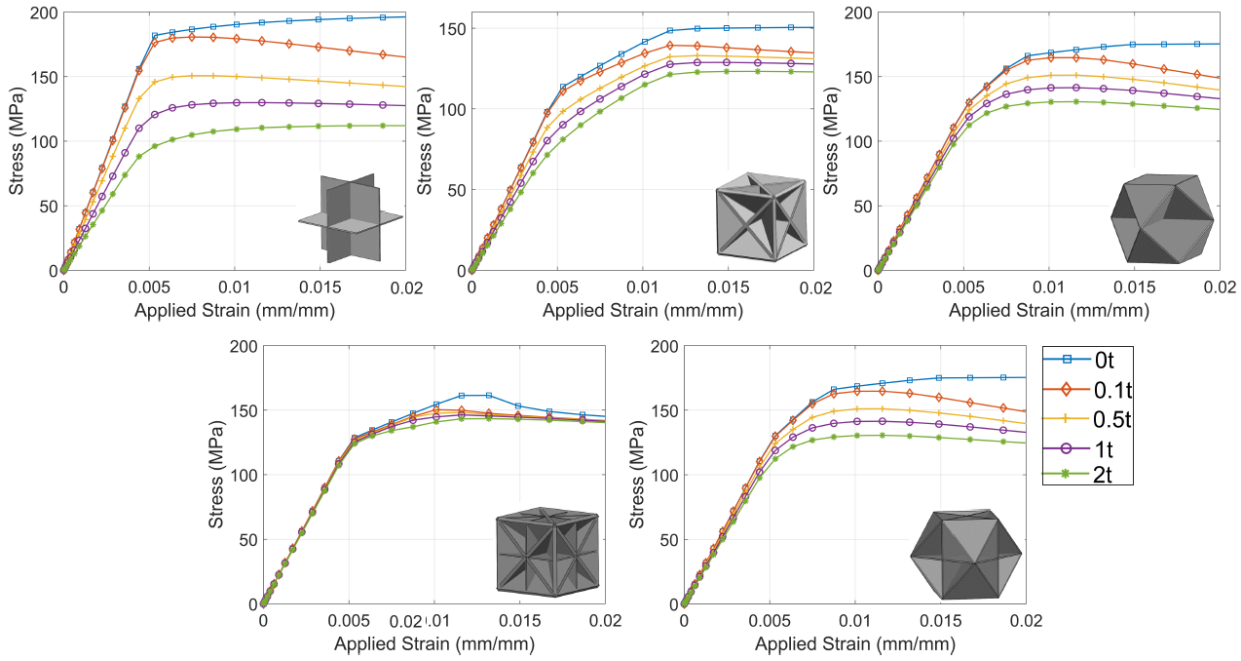

Figure 4: Stress-strain curves for anisotropic SC, BCC, FCC and isotropic SC-BCC, SC-FCC plate-lattices under compression for relative density ρ*=25%.

The governing failure mechanism of these structures is plate yielding followed by rotation of the plate intersections aligned with the loading direction for each geometry, leading to large bending of the plates. Yielding is initiated from the vertical plates which are aligned with the loading direction. Fig. 5 summarizes the von-Mises stress contours at peak load for all geometries for perfect and imperfect (2t) architectures.

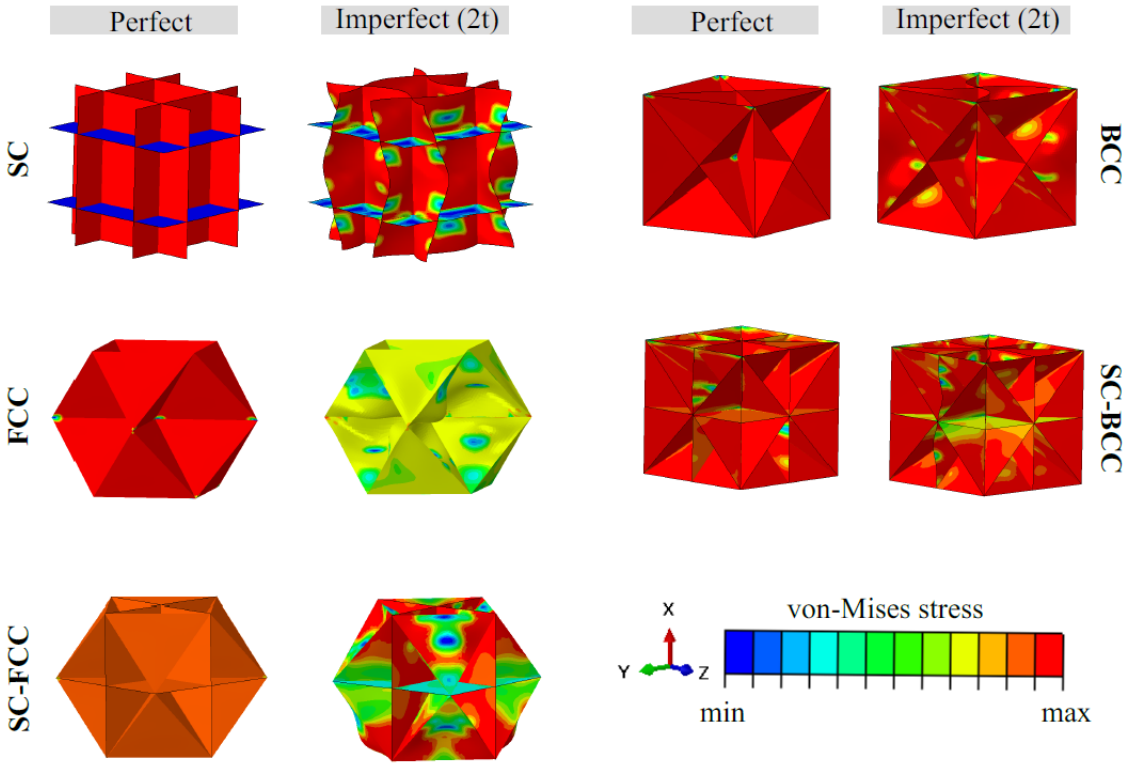

Figure 5: Von-Mises stresses at peak load of each analysis. The lowest (0t) and the highest (2t) imperfections are used for representation. Larger deformations are shown for the imperfect cases at which the deformed shape represents eigenmode 1 and the failures are governed by the yielding and bending of the plates.

Strength results are also summarized in Fig. 6 for all geometries. Knockdown factors calculated as a fraction of strength of imperfect lattices over strength of perfect lattices are depicted against amplitude. The SC plate-lattice is predicted as the most imperfection sensitive plate-lattice geometry for ρ^*=25%, while the SC-BCC is predicted as the least imperfection sensitive geometry. In general, the more braced with plates the plate-lattices of ρ^*=25% are, the less imperfection sensitivity they show in terms of strength.

4.2 Effect of Relative Density

The effect of relative density is assessed herein by varying the relative density of SC plate-lattices between 3% and 25%. Strength knockdown factors are provided in Fig. 7 for all examined relative densities for SC against the respective slenderness ratios (ratios of unit-cell length over plate thickness (L/t) of each relative density). The results show that while SC plate-lattices are imperfection sensitive with their lowest knockdown factors around 0.5 (ρ^*=25%, ρ^*=20%, ρ^*=15%, ρ^*=10%), there are lower-density lattices that are less imperfection sensitive (ρ^*=7%, ρ^*=5%), and most importantly they become imperfection insensitive for low relative densities

(ρ*=3%). In detail, higher densities lead to a trend at which thinner plates (from ρ*=25% to ρ*=10%) resulted to lower knockdowns, while lower relative density ranges (from ρ*=7% to ρ*=3%) resulted to the opposite trend. These different behaviors are attributed to the different failure modes.

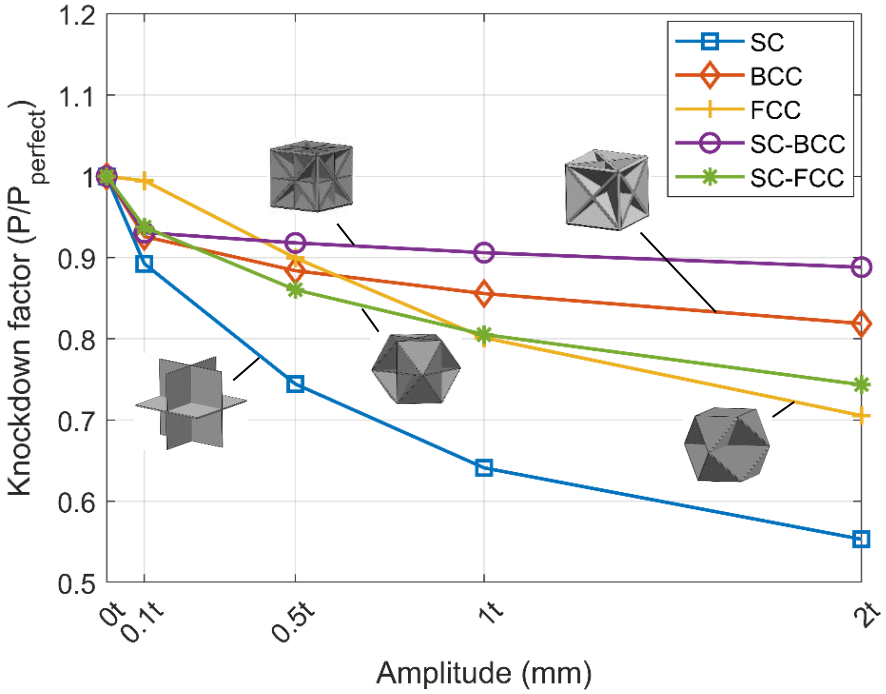

Figure 6: Knockdown factors for all plate-lattices for ρ*=25%. SC is the most imperfection sensitive and SC-BCC is the least imperfection sensitive.

For ρ*=25%-ρ*=10%, plasticity governs the response of the SC plate-lattices and plate large deformation and bending occurs after the peak strength. For ρ*=7%-ρ*=5%, rotation of the top nodes in the plate intersections and buckling of the plates appears before plasticity is reached for the perfect scenarios, while imperfect scenarios are governed by yielding of the plates in the intersections followed by large bending. For ρ*=3%, the load carried by SC-plate-lattices is not affected by the imperfection amplitude due to the buckling of the plates prior to yielding. In detail, for the perfect scenario, high stress concentration in the vertical plates appears initially leading to the rotation of the top intersection nodes and buckling of the vertical plates. As applied strain increases, a buckling mode different from the initial imperfection (inset stress contour shapes in Fig. 7) results before the yielding of the plates. For the imperfect scenarios of SC lattices of ρ*=3%, an elastic buckling mode different than the introduced eigenmode (elastic buckling of the horizontal plates - similarly to the perfect scenarios of the same ρ*=3%) followed by yielding of the plates governs their response.

These results indicate an effort to examine the stability of lower-density plate-lattice materials and provide promising results for potential imperfection insensitive geometries. Examination of lower relative density plate-lattices is a future step of this work aiming to evaluate and understand the behavior of ultra-thin plate-lattices of all geometries (SC, BCC, FCC, SC-BCC, SC-FCC).

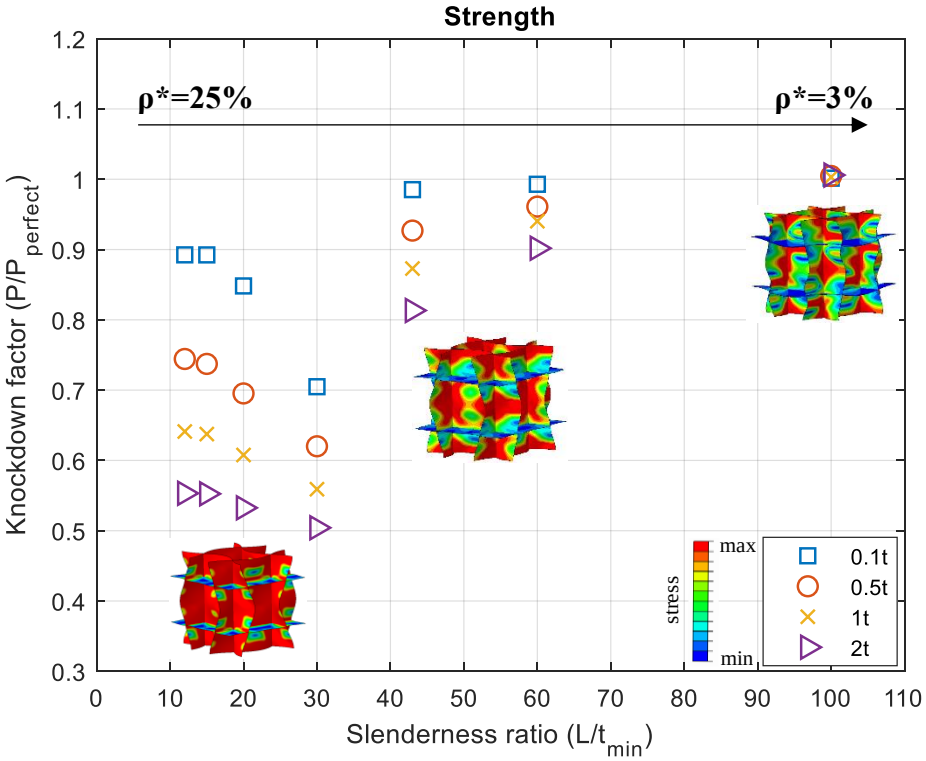

Figure 7: Knockdown factors for SC plate-lattices for various relative densities (ρ*=25%, ρ*=20%, ρ*=15%, ρ*=10%, ρ*=7%, ρ*=5%, ρ*=3%) against plate slenderness ratios. Imperfection sensitivity is reduced or eliminated as ρ* is decreased. Deformed shapes and von-Mises stress contours are also illustrated as inset figures.

5. Conclusions

This work focused on the stability and the impact of geometric imperfections to plate-lattice mechanical metamaterials. Focusing mainly on the strength of SC, BCC, FCC, SC-BCC, SC-FCC lattice structures, strength is evaluated via innovative knockdown factors.

For relative densities of 25%, all plate-lattices (SC, FCC, BCC, SC-FCC, SC-BCC) result to higher strength as imperfection amplitude increases from 0t to 2t (where t is the different minimum thicknesses of all architectures). Yielding and bending of the plates govern the response of all geometries of ρ*=25%. SC is the most imperfection sensitive architecture, while SC-BCC is the least imperfection sensitive geometry. This is mainly attributed to the higher number of plates in SC-BCC geometry that works as braces, although SC-BCC is composed of thinner plates in comparison to SC for the same density.

Expansion of this method to lower relative densities is an immediate goal of this work. In this study, SC-plate lattice behavior is examined over various relative densities within 3% and 25%. Plate-lattices of high relative densities are imperfection sensitive, while low-density plate-lattices behave as imperfection insensitive for the same imperfection amplitudes. The difference in their behavior lies in the yielding and bending dominance in higher relative densities, compared to the elastic buckling of the lower-density plate-lattices prior to yielding of the plates.

Ultra-thin plate-lattice architected materials will be investigated for SC, BCC, FCC, SC-BCC, and SC-FCC with a potential use to enhance stability in structural applications. Since geometric

imperfections are inevitable using 3D printing techniques, new material architectures insensitive to imperfections will improve the design and reliability of structures.

References

Abaqus User, Manual. (2018). "Abaqus Theory Guide. Version 6.14." USA.: Dassault Systems Simulia Corp.

Berger, J. B., Wadley, H. N. G., & McMeeking, R. M. (2017). Mechanical metamaterials at the theoretical limit of isotropic elastic stiffness. *Nature*, 543(7646), 533-537.

Crook, C., Bauer, J., Izard, A. G., de Oliveira, C. S., e Silva, J. M. D. S., Berger, J. B., & Valdevit, L. (2020). Plate-nanolattices at the theoretical limit of stiffness and strength. *Nature communications*, *11*(1), 1-11.

Bonatti, C., & Mohr, D. (2019). Mechanical performance of additively-manufactured anisotropic and isotropic smooth shell-lattice materials: Simulations & experiments. *Journal of the Mechanics and Physics of Solids*, 122, 1-26.

Bonatti, C., & Mohr, D. (2019). Smooth-shell metamaterials of cubic symmetry: anisotropic elasticity, yield strength and specific energy absorption. *Acta Materialia*, 164, 301-321.

Deshpande, V. S., & Fleck, N. A. (2000). High strain rate compressive behaviour of aluminium alloy foams. *International Journal of Impact Engineering*, 24(3), 277-298.

Deshpande, V. S., Ashby, M. F., & Fleck, N. A. (2001). Foam topology: bending versus stretching dominated architectures. *Acta materialia*, 49(6), 1035-1040.

Deshpande, V. S., Fleck, N. A., & Ashby, M. F. (2001). Effective properties of the octet-truss lattice material. *Journal of the Mechanics and Physics of Solids*, *49*(8), 1747-1769.

Elsayed, M. S., & Pasini, D. (2010). Multiscale structural design of columns made of regular octet-truss lattice material. *International Journal of Solids and Structures*, *47*(14-15), 1764-1774.

Gibson, L., Ashby, M., Schajer, G., & Robertson, C. (1982). The Mechanics of Two-Dimensional Cellular Materials. *Proceedings of the Royal Society of London. Series A, Mathematical and Physical Sciences, 382*(1782), 25-42. Retrieved January 9, 2021, from http://www.jstor.org/stable/2397267.

Gibson, L., & Ashby, M. (1982). The Mechanics of Three-Dimensional Cellular Materials. *Proceedings of the Royal Society of London. Series A, Mathematical and Physical Sciences, 382*(1782), 43-59. Retrieved January 9, 2021, from http://www.jstor.org/stable/2397268.

Gross, A., Pantidis, P., Bertoldi, K., & Gerasimidis, S. (2019). Correlation between topology and elastic properties of imperfect truss-lattice materials. *Journal of the Mechanics and Physics of Solids*, *124*, 577-598.

Gu, X. W., & Greer, J. R. (2015). Ultra-strong architected Cu meso-lattices. *Extreme Mechanics Letters*, *2*, 7-14.

Han, S. C., Lee, J. W., & Kang, K. (2015). A new type of low density material: Shellular. *Advanced Materials*, 27(37), 5506-5511.

Han, S. C., & Kang, K. (2019). Another stretching-dominated micro-architectured material, shellular. *Materials Today*, 31, 31-38.

Hashin, Z., & Shtrikman, S. (1963). A variational approach to the theory of the elastic behaviour of multiphase materials. *Journal of the Mechanics and Physics of Solids*, *11*(2), 127-140.

Meza, L. R., Zelhofer, A. J., Clarke, N., Mateos, A. J., Kochmann, D. M., & Greer, J. R. (2015). Resilient 3D hierarchical architected metamaterials. *Proceedings of the National Academy of Sciences*, *112*(37), 11502-11507.

O'Masta, M. R., Dong, L., St-Pierre, L., Wadley, H. N. G., & Deshpande, V. S. (2017). The fracture toughness of octet-truss lattices. *Journal of the Mechanics and Physics of Solids*, *98*, 271-289.

Papka, S. D., & Kyriakides, S. (1999). Biaxial crushing of honeycombs:—Part 1: Experiments. *International Journal of Solids and Structures*, 36(29), 4367-4396.

Tancogne-Dejean, T., Diamantopoulou, M., Gorji, M. B., Bonatti, C., & Mohr, D. (2018). 3D Plate-Lattices: An Emerging Class of Low-Density Metamaterial Exhibiting Optimal Isotropic Stiffness. *Advanced Materials*, 30(45), 1803334.

Tancogne-Dejean, T., Li, X., Diamantopoulou, M., Roth, C. C., & Mohr, D. (2019). High Strain Rate Response of Additively-Manufactured Plate-Lattices: Experiments and Modeling. *Journal of Dynamic Behavior of Materials*, *5*(3), 361-375.